

Anisotropic Neural Representation Learning for High-Quality Neural Rendering

Yifan Wang
SUSTech

wangyf1998sc@foxmail.com

Jun Xu
SUSTech

12232114@mail.sustech.edu.cn

Yuan Zeng [†]
SUSTech

zengy3@sustech.edu.cn

Yi Gong [†]
SUSTech

gongy@sustech.edu.cn

Abstract

Neural radiance fields (NeRFs) have achieved impressive view synthesis results by learning an implicit volumetric representation from multi-view images. To project the implicit representation into an image, NeRF employs volume rendering that approximates the continuous integrals of rays as an accumulation of the colors and densities of the sampled points. Although this approximation enables efficient rendering, it ignores the direction information in point intervals, resulting in ambiguous features and limited reconstruction quality. In this paper, we propose an anisotropic neural representation learning method that utilizes learnable view-dependent features to improve scene representation and reconstruction. We model the volumetric function as spherical harmonic (SH)-guided anisotropic features, parameterized by multilayer perceptrons, facilitating ambiguity elimination while preserving the rendering efficiency. To achieve robust scene reconstruction without anisotropy overfitting, we regularize the energy of the anisotropic features during training. Our method is flexible and can be plugged into NeRF-based frameworks. Extensive experiments show that the proposed representation can boost the rendering quality of various NeRFs and achieve state-of-the-art rendering performance on both synthetic and real-world scenes.

1. Introduction

Neural radiance field (NeRF) [46] models the 3D scene geometry and view-dependent appearance by two cascaded multi-layer perceptrons (MLPs) and uses volume rendering to reconstruct photorealistic novel views. The advent of NeRF has sparked a flurry of work on neural rendering and has opened the way to many applications [4, 15, 18, 76–

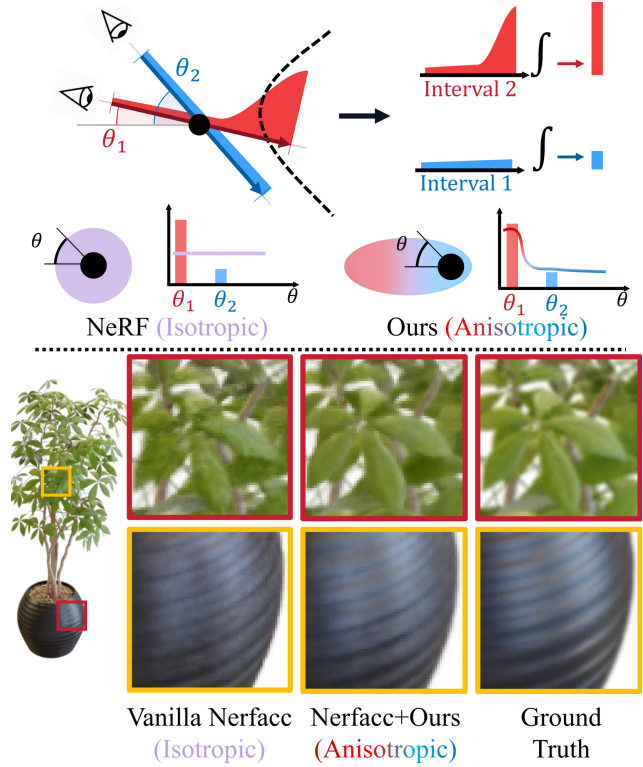


Figure 1. Top: Vanilla NeRF uses point sampling and view-independent functions to estimate σ and e , resulting in directional ambiguity when representing intervals. To eliminate the ambiguity, we introduce anisotropic functions to model the integration along various directions. Bottom: Our anisotropic neural representation enables to assist Nerfacc in capturing more geometric details.

78]. One of the key underpinnings of NeRF is differentiable volume rendering which facilitates learning the MLP-based radiance field solely from a 2D photometric loss on synthesized images in an end-to-end manner. However, NeRF still

[†] Corresponding authors

suffers from blurring and aliasing when reconstructing complex scenes. Specifically, since NeRF is done by sampling a set of points along a ray and approximating the piece-wise continuous integration as an accumulation of the estimated volumetric features of sampled intervals, MLP could only be queried at a fixed discrete set of positions and the same ambiguous point-sampled feature is used to represent the opacity at all points with the interval between two samples, leading to ambiguity in neural rendering. The features of samples can be very different across different rays cast from different viewing directions. Therefore, simultaneously supervising these rays to produce the isotropic volumetric features can result in artifacts like fuzzy surfaces and blurry texture, as shown in Figure 1.

To overcome the limitations of the neural scene representation and enhance rendering quality of NeRF, several works [4–6, 30, 31, 45] introduce shape-based sampling into the scene representation. By embedding novel spatial parameterization schemes, such as Gaussian ellipsoid, frustum, and sphere, into the encoding, these models can reduce representation ambiguity and improve rendering quality with less blurring and aliasing artifacts. However, the representation ambiguities still exist in their radiance fields, since the directional intervals used for rendering are parameterized by the non-directional features. A straightforward solution is to take the viewing direction as input of the first MLP, enabling to represent the scene geometry with view-dependent features. While this method can reduce directional ambiguity in representation, the radiance field is now a high-degree view-dependent function without regularization, and it is prone to overfitting to the appearance of training images but fails to capture the correct geometry [81].

In this paper, we propose a novel radiance field representation to diversify a different model for the density and appearance in neural rendering, leading to better reconstruction of the scene’s geometry and appearance while producing photorealistic novel views. Instead of introducing a different spatial sampling strategy and parameterizing sampled-shapes, we model the density and latent features at a location as view-dependent functions using spherical harmonic (SH) basis. The spherical harmonics can be evaluated at arbitrary query viewing directions to capture anisotropy. Although this can be done by converting an existing NeRF into such anisotropic representations via projection onto the SH basis functions, we simply modify the first MLP in NeRF to predict the geometry explicitly in terms of spherical harmonics, resulting in a compact and generalizable anisotropic neural representation. Specifically, we train the first MLP that produces coefficients for the SH functions instead of the density and latent features. The predicted values can later be directly used for appearance estimation and pixel rendering.

Additionally, training the anisotropic neural representa-

tion using only a color reconstruction loss will cause strong anisotropy and suffer from shape-radiance ambiguity in rendering[81]. Although existing regularization methods, such as Patch-based Consistency [17], warp-based loss [83], depth or multi-view multi-view stereo prior [8, 68, 70, 73] can be a solution, they rely on the geometric prior and structural output and significantly increase the computational cost. We aim to introduce an effective anisotropy regularization according to our SH function-based representation. To this end, we decompose the anisotropic elements from the predicted density and latent features and employ point-wise operation to penalize the anisotropy in the geometry representation. This improves the memory and computational efficiency of our method and allows us to render high-quality novel views. Moreover, our anisotropic neural representation can be used as a sub-model to replace the first MLP in various NeRFs, resulting in anisotropic geometric features and better rendering quality.

We extensively evaluate the effectiveness and generalizability of our anisotropic neural representation on benchmark datasets including both synthetic and real-world scenes. Both quantitative and qualitative comparison results demonstrate that plugging our anisotropic neural representation can further improve the rendering quality of various NeRFs. Our contributions are summarized as follows:

- A novel anisotropic neural representation is proposed to model the scene geometry by view-dependent density and latent features. It effectively reduces directional ambiguity in neural rendering and results in better geometric and appearance reconstruction and rendering quality.
- A modified NeRF network is trained to predict view-dependent geometry in terms of spherical basis functions, which is flexible and generalizable to various existing NeRFs.
- A point-wise anisotropy regularization loss enables highly efficient view-dependent penalties during model training to avoid overfitting.

2. Related Work

Scene representations for Novel view synthesis. Synthesizing views from a novel viewpoint is a long-standing problem in computer vision and computer graphics. Traditional methods typically synthesize novel views from a set of images [11–13, 21, 59] or light fields [37, 63, 72]. Although these methods work well on dense input images, they are limited by the sparse inputs and the quality of 3D reconstruction. To synthesize novel views from a sparse set of images, some methods leverage geometry structure of the scene [26, 53]. Recent advances in deep learning have facilitated the use of neural networks for estimating scene geometry, such as voxel grids [29, 41, 55, 60], point clouds [1, 36, 62, 69], and multi-plane images [19, 84]. Although these discrete representation methods can improve the ren-

dering quality of novel views, the estimation of the scene geometry is not accurate enough for high-resolution scenes.

By modeling the scene geometry and appearance as a continuous volume, neural radiance fields (NeRFs) [46] have achieved state-of-the-art novel synthesis effects. Specifically, NeRF maps the input coordinate to density and radiance scene values and uses volume rendering [43] to synthesize the images. In addition, various schemes have been introduced to improve the robustness of NeRF to few-shot inputs [35, 49, 67, 78], anti-aliasing [4–6, 30], handle dynamics [16, 42, 45, 75] and speed up rendering [14, 23, 47, 65], etc. Our method is more closely related to anti-aliasing NeRFs, which adopt interval-dependent features to assist the MLP in capturing more accurate geometry and reducing blurring artifacts in novel view synthesis. In contrast, we introduce a plug-and-play anisotropic neural representation that enables it to be plugged into various NeRFs to alleviate ambiguity and improve rendering quality.

Anti-ambiguity in neural rendering. Volume rendering is an important technique with a long history of research in the graphics community. Traditional graphics rendering methods include studying ray sampling efficiency and data structures for coarse-to-fine hierarchical sampling. Recent NeRF and its succeeding works have shown impressive results by replacing or augmenting the traditional graphics rendering with neural networks. The volume rendering used in these works is approximated to a discrete accumulation under the assumption of a piece-wise constant opacity and color, enabling to learn the NeRF-based implicit representations. However, the piece-wise constant assumption results in rendering results that are sensitive to the sampled points as well the cumulative density function of the distribution of the sampled interval, introducing ambiguous features and aliasing artifacts in NeRF renderings.

To address these challenges, recent works have explored super-sampling or pre-filtering techniques. Super-sampling is done by casting multiple rays per pixel to approach the Nyquist frequency. Although this strategy works well for eliminating ambiguity, it is computationally expensive. Pre-filtering techniques are more computationally efficient, since the filtered versions of scene content can be pre-computed ahead of time. Recently, pre-filtering has been introduced into neural representation and rendering to reduce ambiguity and aliasing artifacts [9]. Mip-NeRF [4] samples the cone instead of rays to consider the shape and size of the volume viewed by each ray and optimizes a pre-filtered representation of the scene during training. With sampled shape-dependent inputs, the MLP of Mip-NeRF can capture various volumetric features to mitigate ambiguity, resulting in a high-quality multi-scale representation and anti-aliasing. Mip-NeRF 360 [5] extends Mip-NeRF with

a novel distortion-based regularizer to tackle unbounded scenes. Zip-NeRF [6] adopts multi-sampling to approximate a cone with hash encoding. Tri-Mip [30] leverages multi-level 2D mipmaps to model the pre-filtered 3D feature space and projects parameterized spheres on three mipmaps to achieve anti-aliasing encoding. Although the shape and size of volumes at different scales can be fitted by introducing various sampling techniques in NeRF, shape-based features still exist in ambiguity since the non-directional shape intervals are used in accumulation for pixel rendering. Our work draws inspiration from the early work on anisotropic volume rendering [57] and is the first to model scene geometry as an anisotropic neural representation based on spherical harmonics for volume rendering.

3. Preliminaries

Neural Radiance Fields. Given a 3D position \mathbf{x} and a 2D viewing direction \mathbf{d} , NeRF [46] first uses a multilayer perceptron (MLP) parameterized by weights θ to predict the density σ and an intermediate vector \mathbf{e} from the input position \mathbf{x} : $(\sigma, \mathbf{e}) = \mathcal{F}_\theta(\mathbf{x})$. Then, a second MLP parameterized by weights ϕ is employed to estimate the color \mathbf{c} from the direction \mathbf{d} and the vector \mathbf{e} : $\mathbf{c} = \mathcal{F}_\phi(\mathbf{d}, \mathbf{e})$.

Volume Rendering. The color of a pixel in NeRFs can be rendered by casting a ray $\mathbf{r} = \mathbf{o} + t\mathbf{d}$ from the camera origin \mathbf{o} through the pixel along the direction \mathbf{d} , where t is the distance to the origin. The pixel's color value can be computed by integrating colors and densities along a ray based on the volume rendering [43]:

$$\hat{C}(\mathbf{r}) = \int_0^\infty T(t)\sigma(t)\mathbf{c}(t) dt, \quad (1)$$

where $T(t) = \exp\left(-\int_0^t \sigma(\mathbf{r}(s)) ds\right)$ represents occlusions by integrating the differential density between 0 to t .

Since the volume density σ and radiance \mathbf{c} are the outputs of MLPs, NeRF rendering methods approximate this continuous integral using a sampling-based Riemann sum instead [56]. Within the near and far bounds, t_n and t_f of the cast ray, a subset of points on the ray is sampled in a near-to-far order. Let $\mathbf{t}_N = t_1, \dots, t_N$ be N samples on the ray that define the intervals, e.g., $I_i = [t_i, t_{i+1}]$ is the i th interval, and $I_0 = [0, t_1]$, $I_N = [t_N, \infty]$. The volume density for particles along the interval I_i is predicted under the assumption that opacity is constant along each interval, which indicates $\sigma_t = \sigma_{t_i}, \forall t \in [t_i, t_{i+1}]$ for particles of constant radius and material. We denote $\sigma_{t_i} = \sigma_i$ for notation convenience. Under this assumption, the rendered color can be written as an approximation of the N sampled points:

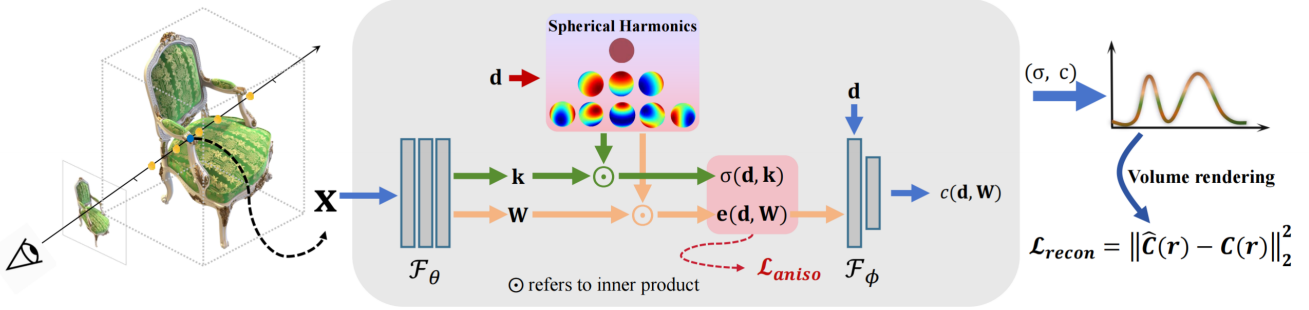


Figure 2. Overview of our anisotropic neural representation. In contrast to output isotropic σ and e directly as in vanilla NeRF, we composite anisotropic features by learning the SH coefficients predicted from MLP \mathcal{F}_θ . During training, the model is optimized end-to-end by minimizing a joint loss of \mathcal{L}_{recon} and \mathcal{L}_{aniso} .

$$\begin{aligned} \hat{C}(\mathbf{r}) &= \sum_{i=0}^N \left(\int_{t_i}^{t_{i+1}} T(u) \sigma(u) du \right) c_i \\ &= \sum_{i=0}^N T_i (1 - \exp(-\sigma_i(t_{i+1} - t_i))) c_i, \end{aligned} \quad (2)$$

where $T_i = \exp\left(-\sum_{j=1}^{i-1} \sigma_j(t_{j+1} - t_j)\right)$ represents the transmittance accumulated along the ray until the i th sample. For more detailed derivation, please refer to [44]. The NeRF model is optimized by minimizing the L_2 reconstruction loss between the ground truth and synthesized images, which can be expressed as follows:

$$\mathcal{L}_{recon} = \frac{1}{|\mathcal{R}|} \sum_{\mathbf{r} \in \mathcal{R}} \left\| \hat{C}(\mathbf{r}) - C(\mathbf{r}) \right\|_2^2, \quad (3)$$

where \mathcal{R} is a set of rays sampled during training, and C is the ground truth pixel color value.

Limitations. While images can be efficiently rendered using NeRF renderings, it is non-trivial to represent an anisotropic surface with the predicted density and the recovered geometry is far from satisfactory. In addition, leveraging the same predicted density to represent the distribution along the interval between two samples can hardly capture the correct geometry of different rays cast from different directions. Moreover, approximating the continuous integral of the interval as an accumulation of the isotropic features of sampled points has no guarantee for correct approximation. Figure 1 shows that the vanilla NeRF using an isotropic representation has limited rendering quality and suffers from blurring artifacts. This insight motivates our anisotropic neural representation.

4. Method

Given a set of scenes with a collection of images and their camera parameters, we aim to learn an anisotropic neural representation for high-quality neural rendering. In this section, we first represent the scene geometry and appearance using spherical harmonic-based implicit representations to capture anisotropy of surfaces (Sec. 4.1). Then we introduce an anisotropy regularization to encourage a sparse anisotropic neural representation and summarize our overall training procedure (Sec. 4.2).

4.1. Anisotropic Neural Representation

Figure 2 illustrates an overview of our method. While vanilla NeRF takes a 3D position \mathbf{x} as an input of a density MLP \mathcal{F}_θ to estimate the scene geometry, including volume density σ and latent feature e , we leverage both the 3D position and 2D viewing direction to introduce anisotropic features to represent the scene geometry. Although naively embedding the direction d into the density MLP \mathcal{F}_θ can realize anisotropic implicit geometry representation, this design will directly increase the dimension of input data and cause the model more easily fit the training data and estimate incorrect scene geometry [81]. To capture anisotropy in scene representation, our method utilizes spherical harmonics (SH), which have been used to model Lambertian surfaces [7, 54], or even glossy surfaces [61]. We query the SH functions $Y_l^m: \mathbb{S}^2 \mapsto \mathbb{R}$ at a viewing direction d and then fit the anisotropic geometry representations by finding the corresponding coefficients. We use low-degree SH functions to compute ideal values of view-independent density and latent components, and high-degree SH functions for view-dependent components.

For any sampled point \mathbf{x} in the space, we adapt \mathcal{F}_θ to estimate the spherical harmonic coefficients \mathbf{k} and \mathbf{W} , rather than the volume density and latent feature:

$$(\mathbf{k}, \mathbf{W}) = \mathcal{F}_\theta(\mathbf{x}), \quad (4)$$

where the spherical harmonic coefficients $\mathbf{k} = (k_l^m)_{l:0 \leq l \leq L}^{m:-l \leq m \leq l}$ is related to calculate the view-dependent volume density and $\mathbf{W} = [\mathbf{w}_1, \dots, \mathbf{w}_K]^\top$ consists of K sets of SH coefficients that used to determine the K -dimensional latent feature vector. For $n \in \{1, \dots, K\}$, we have $\mathbf{w}_n = (w_{nl}^m)_{l:0 \leq l \leq L}^{m:-l \leq m \leq l}$. For \mathbf{k} or \mathbf{w}_n , there are $(L+1)^2$ spherical harmonics of degree at the most L . The view-dependent density σ and latent feature \mathbf{e} at position \mathbf{x} are then determined by querying the SH functions Y_l^m at the desired viewing direction \mathbf{d} :

$$\sigma(\mathbf{d}, \mathbf{k}) = \sum_{l=0}^L \sum_{m=-l}^l k_l^m Y_l^m(\mathbf{d}), \quad (5)$$

and

$$e_n(\mathbf{d}, \mathbf{w}_n) = \sum_{l=0}^L \sum_{m=-l}^l w_{nl}^m Y_l^m(\mathbf{d}). \quad (6)$$

The equations (5) and (6) can be seen as the factorization of the density and latent feature with the isotropic and anisotropic SH basis functions, respectively. This eliminates the input of view direction to the density MLP and enables efficient generation of view-dependent geometry features. Then, a color MLP takes the inputs of the estimated latent feature $\mathbf{e}(\mathbf{d}, \mathbf{W})$ and the direction \mathbf{d} to predict the color value \mathbf{c} :

$$\mathbf{c}(\mathbf{d}, \mathbf{W}) = \mathcal{F}_\phi(\mathbf{d}, \mathbf{e}(\mathbf{d}, \mathbf{W})). \quad (7)$$

Given the estimated volume density $\sigma(\mathbf{d}, \mathbf{k})$ and color value $\mathbf{c}(\mathbf{d}, \mathbf{W})$, a pixel color $\hat{C}(\mathbf{r})$ in the radiance field along the ray \mathbf{r} can be predicted using the volume rendering in equation (2). Note that since the proposed scene geometry representation only adapts the original density MLP to learn SH coefficients and efficiently convert the input position into anisotropic features, making it easy to be plugged into various existing NeRF-based scene representation models and assists the models in capturing more precise geometries for high-quality novel view synthesis.

4.2. Training

NeRF adopts pixel-wise RGB reconstruction loss \mathcal{L}_{recon} to optimize view-independent geometry density and view-dependent color for scene reconstruction. However, it is difficult to optimize a correct geometry purely from the input RGB images, especially when view-dependent components are used in the geometry representation, since a high degree of anisotropy will be learned to fit the training images, leading to shape-radiance ambiguity and the degradation of rendering quality. To facilitate robust mapping under our anisotropic neural representation, we propose a point-wise anisotropy constraint, which penalizes the anisotropy of the model to mitigate shape-radiance ambiguity efficiently.

Anisotropy Regularization. Without any regularization, the model is free to fit a set of training images by exploiting view-dependent anisotropic neural representation rather than recover the correct geometry. The representation with strong anisotropy would generate shape-radiance ambiguity, resulting in blurring artifacts and incorrect geometries in rendering novel test views. We therefore introduce a new regularization method that suppresses the anisotropy in geometry representations.

To apply regularization techniques for penalizing anisotropy, we first define the anisotropic features according to the SH basis functions. Since the 0-degree SH function $Y_0^0(\mathbf{d})$ is view-independent, we remove the view-independent component from the estimated density $\sigma(\mathbf{d}, \mathbf{k})$ and latent feature $\mathbf{e}(\mathbf{d}, \mathbf{W})$ to compute the view-dependent component:

$$\sigma^{aniso}(\mathbf{d}, \mathbf{k}) = \sum_{l=1}^L \sum_{m=-l}^l k_l^m Y_l^m(\mathbf{d}), \quad (8)$$

and

$$e_n^{aniso}(\mathbf{d}, \mathbf{w}_n) = \sum_{l=1}^L \sum_{m=-l}^l w_{nl}^m Y_l^m(\mathbf{d}). \quad (9)$$

We formulate our anisotropy regularization loss as:

$$\mathcal{L}_{aniso} = \frac{1}{N} \sum_{i=1}^N \left(\|\sigma^{aniso}(\mathbf{d}_i, \mathbf{k}_i)\|_2^2 + \|e^{aniso}(\mathbf{d}_i, \mathbf{W}_i)\|_2^2 \right), \quad (10)$$

where \mathbf{d}_i , \mathbf{k}_i and \mathbf{W}_i represent the direction, density-related SH coefficients and latent feature-related SH coefficients at the i th point sampled on ray \mathbf{r} , respectively.

Full Objective Loss. To learn the high-fidelity scene reconstruction, we optimize the following total loss in each iteration:

$$\mathcal{L} = \mathcal{L}_{recon} + \lambda \mathcal{L}_{aniso}, \quad (11)$$

where λ is a hyperparameter to scale the anisotropy regularization loss. In addition, to plug our anisotropy neural representation in different existing NeRFs for novel view synthesis, we remain the original losses and add the anisotropy regularization loss \mathcal{L}_{aniso} in the full objective loss for model training.

5. Experiments

In this section, we evaluate the effectiveness and generalizability of our method on novel view synthesis. We plug our anisotropic neural representation into existing state-of-the-art NeRFs and present quantitative and qualitative comparisons between the baseline NeRFs and our models on both synthetic and real-world benchmark datasets in Sec. 5.1. A comprehensive ablation study that supports our design

	Blender				Shiny Blender			
	PSNR↑	SSIM↑	LPIPS↓	Avg.↓	PSNR↑	SSIM↑	LPIPS↓	Avg.↓
Nerfacc	33.06	0.961	0.053	0.017	30.76	0.933	0.126	0.030
Nerfacc+Ours	34.08	0.966	0.046	0.015	31.75	0.943	0.122	0.027
K-planes	32.34	0.962	0.052	0.018	30.93	0.943	0.120	0.028
K-planes+Ours	33.00	0.964	0.052	0.017	31.65	0.948	0.103	0.025
Tri-mip	33.78	0.963	0.051	0.016	31.66	0.941	0.115	0.027
Tri-mip+Ours	34.69	0.965	0.049	0.015	32.04	0.941	0.114	0.026

Table 1. Quantitative results on Blender and Shiny Blender. Our representation significantly improves the numerical performance of the three baselines on synthetic scenes.

choices is also provided in Sec. 5.2. More details and per-scene results are provided in our supplementary materials.

Datasets and metrics We report our results on three datasets: Blender [46], Shiny Blender [66], and Mip-360 [5]. Blender consists of eight synthetic scenes (*lego, chair, hotdog, ficus, drums, materials, mic, and ship*), where each has 400 synthesized images. Shiny Blender consists of six different glossy objects with more challenging material properties and reflective highlights. We use a subset of five scenes (*car, teapot, toaster, helmet, coffee*) in our experiments. Mip-360 is an unbounded real-world dataset including three outdoor scenes (*garden, bicycle, stump*) and four indoor scenes (*room, kitchen, bonsai, counter*), and each scene contains a complex central object or region along with intricate background details. We follow the default split in [5] to produce training and testing views. In addition, we follow previous NeRF methods and report our quantitative results in terms of peak signal-to-noise ratio (PSNR), structural similarity index (SSIM) [71], learning perceptual image patch similarity (LPIPS) [82] and an average error (Avg.) [4] which summarizes three above metrics.

Baselines. We adopt the following four recently proposed neural rendering methods as baselines: two point-sampling methods Nerfacc [38] and K-Planes [22], and two shape-sampling methods Tri-mipRF [30] and Zip-NeRF [6]. We use the official implementation of Nerfacc, K-Planes, Tri-mipRF and retrain the three models on the Blender and Shiny Blender datasets. As no official code is available, we use an open-source code of Zip-NeRF[64] and retrain Zip-NeRF and Nerfacc on Mip-360. We include two variations of Zip-NeRF as baseline methods in our comparisons: a single-sampling-based Zip-NeRF (S-Zip-NeRF) and a multi-sampling-based Zip-NeRF (M-Zip-NeRF) which samples 6 points to represent an interval.

Implementation Details. For our anisotropic neural representation, we set the maximal degree of spherical harmonic basis $L = 3$ and the hyperparameter $\lambda = 1e - 4$. To keep the dimension of the predicted density σ and latent feature e the same as the baselines, we modify the output dimension of the first MLP \mathcal{F}_θ of the baselines to $(L + 1)^2$ times the original output dimension. We keep other settings the same as our baselines. In addition, we use Nerfacc as our implementation backbone to verify our design choices in ablation studies.

	PSNR↑	SSIM↑	LPIPS↓	Avg.↓
Nerfacc	27.47	0.771	0.294	0.063
Nerfacc+Ours	28.32	0.782	0.281	0.058
S-Zip-NeRF	28.46	0.831	0.282	0.055
S-Zip-NeRF+Ours	28.64	0.836	0.274	0.053
M-Zip-NeRF	28.67	0.838	0.270	0.053
M-Zip-NeRF+Ours	28.97	0.845	0.262	0.051

Table 2. Quantitative comparison results on Mip-360 dataset. Using our representation, the baseline models can achieve better rendering quality.

5.1. Comparisons

Quantitative Comparison. Quantitative results on Blender and Shiny Blender are reported in Table 1. We observe that our representation can significantly improve numerical performance of the three baselines Nerfacc, K-planes and Tri-mip. Quantitative results on Mip-360 are summarized in Table 2. We see our representation also effective for real-world scenes. Specifically, our method can improve the rendering quality of the single-sampling-based Zip-NeRF, resulting in comparable metrics to multi-sampling-based Zip-NeRF, which samples 6 points per interval for anti-aliasing. In addition, our method also brings performance improvements to multi-sampling-based

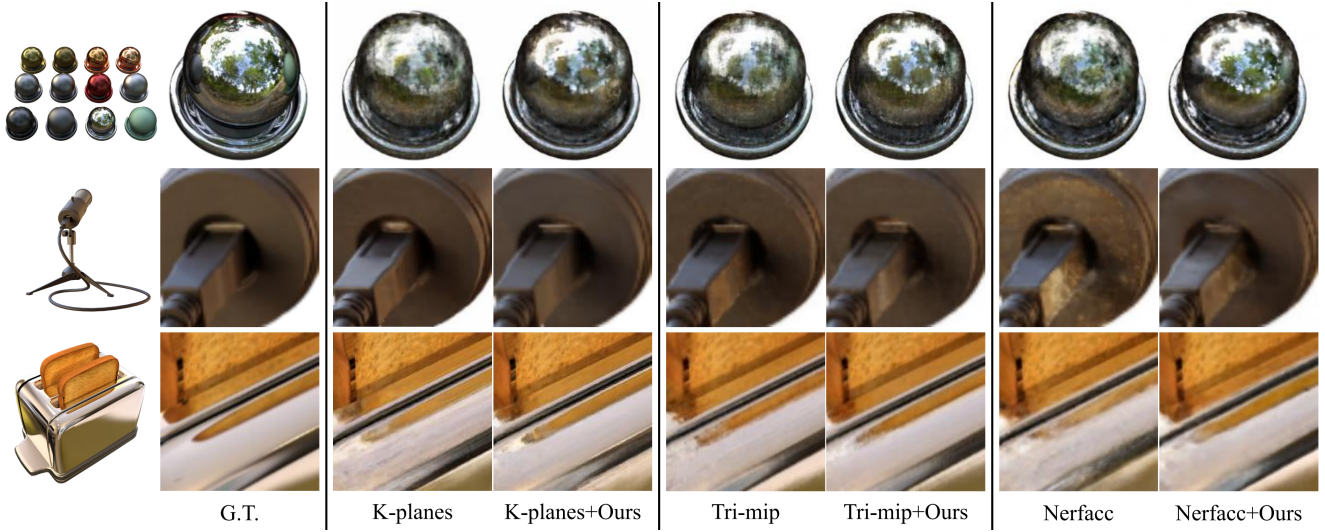


Figure 3. Visual comparison of our method with baselines K-planes [22], Tri-mip [30] and Nerfacc [38] on synthetic scenes. Our representation works well on the three baselines, enabling to reduce blurring and artifacts and reconstruct better geometry and appearance on challenging details.

Zip-NeRF, which indicates that our method can be used in combination with multi-sampling techniques to achieve further better rendering details.

Qualitative Comparison. Figure 3 shows the visual comparison results of three synthetic scenes, including *Material* and *Mic* scenes in Blender and *toaster* in Shiny Blender. It shows that our method can assist the baseline models in recovering the finer appearance and geometric details with less artifacts and blur, such as reflections of *Material* and *toaster* and smooth texture of *Mic*. The rendering results of real-world scenes are illustrated in Figure 4 and Figure 5. As shown in Figure 4, although the vanilla Nerfacc can reconstruct the overall scene geometry well, the tiny objects and local textures are blurry. Our method can help the model capture more geometric details like the lock holes and the potted plants in the *Garden*, and generate better appearance, such as cleaner leaves and plates in the *room*. Figure 5 shows that Zip-NeRF renders photo-realistic images but fails to reconstruct some challenging small structures like banners of *bicycle* and grasses of *stump*. Our method can improve visual performance of both variants of Zip-NeRF, producing sharper and more accurate renderings.

5.2. Ablation Study

Anisotropic neural representation. We first verify the effectiveness of our anisotropic neural representation. In Table 3, we compare our proposed representation to two variations and a baseline (*Nerfacc*). The first one (*Nerfacc+aniso- σ*) is to replace the anisotropic latent fea-

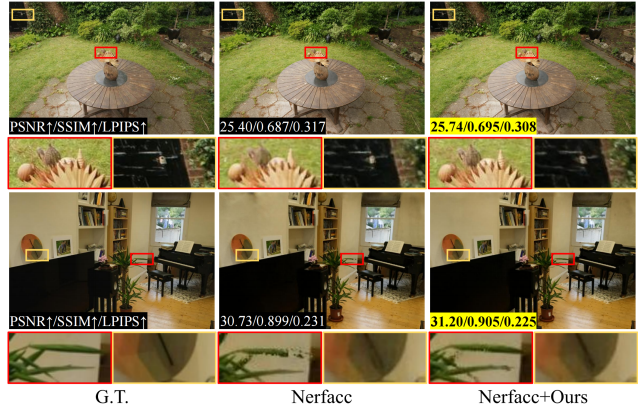


Figure 4. Qualitative comparison of our method with Nerfacc on Mip-360. Our method enhances the rendering quality of vanilla Nerfacc, capturing more geometric details and producing more correct structure and texture.

ture $e(d, W)$ with isotropic one e and uses only anisotropic density $\sigma(d, k)$. This change with anisotropic density can improve the rendering quality of the vanilla Nerfacc but it leads to large performance drops on all metrics compared to our design, showing the necessity of having the anisotropic latent feature for rendering. The second one (*Nerfacc+aniso-e*) is to replace the anisotropic density $\sigma(d, k)$ with the isotropic density σ and uses only the anisotropic latent feature $e(d, W)$. Although this also enhances the rendering quality of the vanilla Nerfacc, it produces inferior performance than our overall design, in-

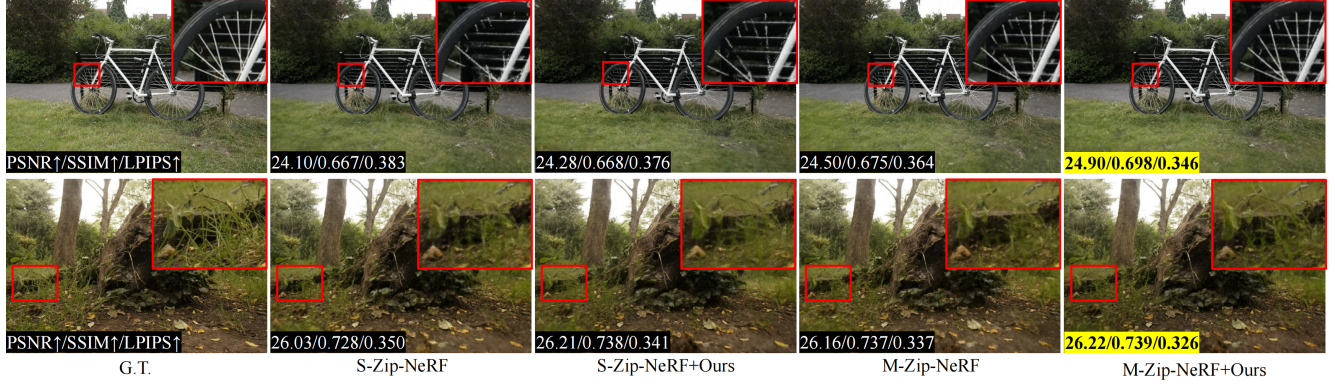


Figure 5. Qualitative comparison of our method with Zip-NeRF on Mip-360. For both variants S-Zip-NeRF and M-Zip-NeRF, our method enables them to estimate opacity more precisely and reconstructs finer details.

	Blender		Mip-360	
	PSNR↑	SSIM↑	PSNR↑	SSIM↑
Nerfacc	33.06	0.961	27.47	0.771
Nerfacc+aniso- σ	33.41	0.961	28.07	0.774
Nerfacc+aniso-e	33.57	0.963	28.21	0.779
Nerfacc+Ours	34.08	0.966	28.32	0.782

Table 3. Quantitative ablation study of the design choices of our anisotropic neural representation on Mip-360 and Blender.

dicating that the anisotropic density can indeed help to learn geometry better. Additionally, The second variation (*Nerfacc+aniso-e*) yields a slightly better numerical performance than the first variation (*Nerfacc+aniso- σ*), this can be explained by the fact that the dimension of the anisotropic latent feature $e(\mathbf{d}, \mathbf{W})$ is higher than the density $\sigma(\mathbf{d}, \mathbf{k})$, which brings more performance gains.

Maximal Degree of SH basis. In Figure 6, we show the impact of the maximal degree of SH basis on rendering quality in terms of PSNR and LPIPS. Our model is the same as vanilla Nerfacc when setting $L = 0$. Our model gets the best rendering quality when setting $L = 3$ on Blender and $L = 4$ on Mip-360, since higher maximal degree more anisotropy can be captured by SH functions but continuously increasing the maximal degree will lead to anisotropy over-fitting and can hardly be interpolated accurately. Meanwhile, the computation complexity of SH functions ($O(L^2)$) increases exponentially as L increases. We set $L = 3$ in our experiments.

Anisotropy regularization. We investigate the impact of anisotropy regularization in Figure 7. Our method bene-

fits more from a larger λ in terms of PSNR and LPIPS across two datasets, with $\lambda = 1e - 4$ being the best. Note that \mathcal{L}_{aniso} is disabled when $\lambda = 0$. When $\lambda \geq 1e - 3$, the rendering quality decreases. Because the overly strong anisotropy penalization leads to limited anisotropy in representation. In our experiments, we set $\lambda = 1e - 4$ to balance anisotropy capturing and overfitting.

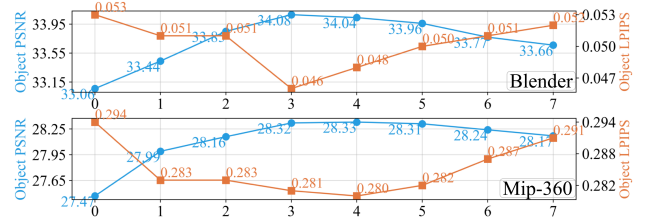


Figure 6. The impact of the maximal degree of SH functions on rendering quality in terms of PSNR and LPIPS. The x -axis refers to the maximal SH degree L .

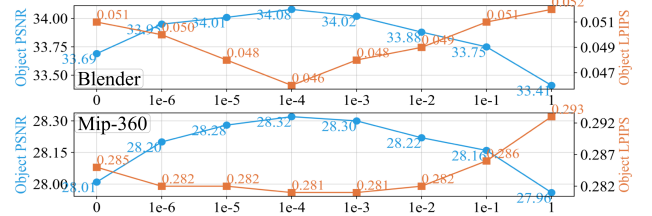


Figure 7. The effect of the strength of anisotropy regularization λ on rendering quality. The x -axis refers to λ .

6. Conclusion

We introduced a novel anisotropic neural representation for NeRFs using spherical harmonic (SH) functions, which enables accurate representation and novel view rendering in complex scenes. We used SH functions and the corresponding coefficients that estimated by a modified NeRF MLP to determine the anisotropic features. During training, an anisotropy regularization is introduced to alleviate the anisotropy overfitting problem. We showed that our design results in a simple and flexible representation module that is easy to generalize to various NeRFs. Experiments on both synthetic and real-world datasets demonstrated the effectiveness of our method on improving the rendering quality for NeRFs.

References

- [1] Panos Achlioptas, Olga Diamanti, Ioannis Mitliagkas, and Leonidas Guibas. Learning representations and generative models for 3d point clouds. In *International conference on machine learning*, pages 40–49. PMLR, 2018. [2](#)
- [2] Abien Fred Agarap. Deep learning using rectified linear units (relu). *arXiv preprint arXiv:1803.08375*, 2018.
- [3] Young Chun Ahn, Seokhwan Jang, Sungheon Park, Ji-Yeon Kim, and Nahyup Kang. Panerf: Pseudo-view augmentation for improved neural radiance fields based on few-shot inputs. *arXiv preprint arXiv:2211.12758*, 2022.
- [4] Jonathan T Barron, Ben Mildenhall, Matthew Tancik, Peter Hedman, Ricardo Martin-Brualla, and Pratul P Srinivasan. Mip-nerf: A multiscale representation for anti-aliasing neural radiance fields. In *Proceedings of the IEEE/CVF International Conference on Computer Vision*, pages 5855–5864, 2021. [1, 2, 3, 6](#)
- [5] Jonathan T Barron, Ben Mildenhall, Dor Verbin, Pratul P Srinivasan, and Peter Hedman. Mip-nerf 360: Unbounded anti-aliased neural radiance fields. In *Proceedings of the IEEE/CVF Conference on Computer Vision and Pattern Recognition*, pages 5470–5479, 2022. [3, 6](#)
- [6] Jonathan T Barron, Ben Mildenhall, Dor Verbin, Pratul P Srinivasan, and Peter Hedman. Zip-nerf: Anti-aliased grid-based neural radiance fields. *arXiv preprint arXiv:2304.06706*, 2023. [2, 3, 6](#)
- [7] Ronen Basri and David W Jacobs. Lambertian reflectance and linear subspaces. *IEEE transactions on pattern analysis and machine intelligence*, 25(2):218–233, 2003. [4](#)
- [8] Wenjing Bian, Zirui Wang, Kejie Li, Jia-Wang Bian, and Victor Adrian Prisacariu. Nope-nerf: Optimising neural radiance field with no pose prior. In *Proceedings of the IEEE/CVF Conference on Computer Vision and Pattern Recognition*, pages 4160–4169, 2023. [2](#)
- [9] Ralph Beebe Blackman and John Wilder Tukey. The measurement of power spectra from the point of view of communications engineering—part i. *Bell System Technical Journal*, 37(1):185–282, 1958. [3](#)
- [10] James F Blinn. Models of light reflection for computer synthesized pictures. In *Proceedings of the 4th annual conference on Computer graphics and interactive techniques*, pages 192–198, 1977.
- [11] Chris Buehler, Michael Bosse, Leonard McMillan, Steven Gortler, and Michael Cohen. Unstructured lumigraph rendering. In *Seminal Graphics Papers: Pushing the Boundaries, Volume 2*, pages 497–504. 2023. [2](#)
- [12] Gaurav Chaurasia, Sylvain Duchene, Olga Sorkine-Hornung, and George Drettakis. Depth synthesis and local warps for plausible image-based navigation. *ACM Transactions on Graphics (TOG)*, 32(3):1–12, 2013.
- [13] Gaurav Chaurasia, Olga Sorkine, and George Drettakis. Silhouette-aware warping for image-based rendering. In *Computer Graphics Forum*, volume 30, pages 1223–1232. Wiley Online Library, 2011. [2](#)
- [14] Anpei Chen, Zexiang Xu, Andreas Geiger, Jingyi Yu, and Hao Su. Tensorf: Tensorial radiance fields. In *European Conference on Computer Vision*, pages 333–350. Springer, 2022. [3](#)
- [15] Anpei Chen, Zexiang Xu, Fuqiang Zhao, Xiaoshuai Zhang, Fanbo Xiang, Jingyi Yu, and Hao Su. Mvsnerf: Fast generalizable radiance field reconstruction from multi-view stereo. In *Proceedings of the IEEE/CVF International Conference on Computer Vision*, pages 14124–14133, 2021. [1](#)
- [16] Xingyu Chen, Qi Zhang, Xiaoyu Li, Yue Chen, Ying Feng, Xuan Wang, and Jue Wang. Hallucinated neural radiance fields in the wild. In *Proceedings of the IEEE/CVF Conference on Computer Vision and Pattern Recognition*, pages 12943–12952, 2022. [3](#)
- [17] Zheng Chen, Chen Wang, Yuan-Chen Guo, and Song-Hai Zhang. Structnerf: Neural radiance fields for indoor scenes with structural hints. *IEEE Transactions on Pattern Analysis and Machine Intelligence*, 2023. [2](#)
- [18] Zhiqin Chen, Thomas Funkhouser, Peter Hedman, and Andrea Tagliasacchi. Mobilenerf: Exploiting the polygon rasterization pipeline for efficient neural field rendering on mobile architectures. In *Proceedings of the IEEE/CVF Conference on Computer Vision and Pattern Recognition*, pages 16569–16578, 2023. [1](#)
- [19] Inchang Choi, Orazio Gallo, Alejandro Troccoli, Min H Kim, and Jan Kautz. Extreme view synthesis. In *Proceedings of the IEEE/CVF International Conference on Computer Vision*, pages 7781–7790, 2019. [2](#)
- [20] Tristan Craddick. Improved ray tracing performance through tri-adaptive sampling. 2020.
- [21] Paul E Debevec, Camillo J Taylor, and Jitendra Malik. Modeling and rendering architecture from photographs: A hybrid geometry-and image-based approach. In *Seminal Graphics Papers: Pushing the Boundaries, Volume 2*, pages 465–474. 2023. [2](#)
- [22] Sara Fridovich-Keil, Giacomo Meanti, Frederik Rahbæk Warburg, Benjamin Recht, and Angjoo Kanazawa. K-planes: Explicit radiance fields in space, time, and appearance. In *Proceedings of the IEEE/CVF Conference on Computer Vision and Pattern Recognition*, pages 12479–12488, 2023. [6, 7](#)
- [23] Sara Fridovich-Keil, Alex Yu, Matthew Tancik, Qinzhong Chen, Benjamin Recht, and Angjoo Kanazawa. Plenoxels:

- Radiance fields without neural networks. In *Proceedings of the IEEE/CVF Conference on Computer Vision and Pattern Recognition*, pages 5501–5510, 2022. 3
- [24] Alban Gauthier, Robin Faury, Jérémie Levallois, Théo Thonat, Jean-Marc Thiery, and Tamy Boubekeur. Mipnet: Neural normal-to-anisotropic-roughness mip mapping. *ACM Transactions on Graphics*, 41(6):1–12, 2022.
- [25] Ross Girshick. Fast r-cnn. In *Proceedings of the IEEE international conference on computer vision*, pages 1440–1448, 2015.
- [26] Michael Goesele, Jens Ackermann, Simon Fuhrmann, Carsten Haubold, Ronny Klowsky, Drew Steedly, and Richard Szeliski. Ambient point clouds for view interpolation. In *ACM SIGGRAPH 2010 papers*, pages 1–6. 2010. 2
- [27] Kang Han and Wei Xiang. Multiscale tensor decomposition and rendering equation encoding for view synthesis. In *Proceedings of the IEEE/CVF Conference on Computer Vision and Pattern Recognition*, pages 4232–4241, 2023.
- [28] W Keith Hastings. Monte carlo sampling methods using markov chains and their applications. 1970.
- [29] Tong He, John Collomosse, Hailin Jin, and Stefano Soatto. Deepvoxels++: Enhancing the fidelity of novel view synthesis from 3d voxel embeddings. In *Proceedings of the Asian Conference on Computer Vision*, 2020. 2
- [30] Wenbo Hu, Yuling Wang, Lin Ma, Bangbang Yang, Lin Gao, Xiao Liu, and Yuwen Ma. Tri-miprf: Tri-mip representation for efficient anti-aliasing neural radiance fields. In *Proceedings of the IEEE/CVF International Conference on Computer Vision*, pages 19774–19783, 2023. 2, 3, 6, 7
- [31] Brian KS Isaac-Medina, Chris G Willcocks, and Toby P Breckon. Exact-nerf: An exploration of a precise volumetric parameterization for neural radiance fields. In *Proceedings of the IEEE/CVF Conference on Computer Vision and Pattern Recognition*, pages 66–75, 2023. 2
- [32] James T Kajiya. Anisotropic reflection models. In *Proceedings of the 12th annual conference on Computer graphics and interactive techniques*, pages 15–21, 1985.
- [33] James T Kajiya and Brian P Von Herzen. Ray tracing volume densities. *ACM SIGGRAPH computer graphics*, 18(3):165–174, 1984.
- [34] Bernhard Kerbl, Georgios Kopanas, Thomas Leimkühler, and George Drettakis. 3d gaussian splatting for real-time radiance field rendering. *ACM Transactions on Graphics (ToG)*, 42(4):1–14, 2023.
- [35] Mijeong Kim, Seonguk Seo, and Bohyung Han. Infonerf: Ray entropy minimization for few-shot neural volume rendering. In *Proceedings of the IEEE/CVF Conference on Computer Vision and Pattern Recognition*, pages 12912–12921, 2022. 3
- [36] Hoang-An Le, Thomas Mensink, Partha Das, and Theo Gevers. Novel view synthesis from single images via point cloud transformation. *arXiv preprint arXiv:2009.08321*, 2020. 2
- [37] Marc Levoy and Pat Hanrahan. Light field rendering. In *Seminal Graphics Papers: Pushing the Boundaries, Volume 2*, pages 441–452. 2023. 2
- [38] Rui long Li, Hang Gao, Matthew Tancik, and Angjoo Kanazawa. Nerfacc: Efficient sampling accelerates nerfs. *arXiv preprint arXiv:2305.04966*, 2023. 6, 7
- [39] David B Lindell, Julien NP Martel, and Gordon Wetzstein. Autoint: Automatic integration for fast neural volume rendering. In *Proceedings of the IEEE/CVF Conference on Computer Vision and Pattern Recognition*, pages 14556–14565, 2021.
- [40] Lingjie Liu, Jiatao Gu, Kyaw Zaw Lin, Tat-Seng Chua, and Christian Theobalt. Neural sparse voxel fields. *Advances in Neural Information Processing Systems*, 33:15651–15663, 2020.
- [41] Stephen Lombardi, Tomas Simon, Jason Saragih, Gabriel Schwartz, Andreas Lehrmann, and Yaser Sheikh. Neural volumes: Learning dynamic renderable volumes from images. *arXiv preprint arXiv:1906.07751*, 2019. 2
- [42] Ricardo Martin-Brualla, Noha Radwan, Mehdi SM Sajjadi, Jonathan T Barron, Alexey Dosovitskiy, and Daniel Duckworth. Nerf in the wild: Neural radiance fields for unconstrained photo collections. In *Proceedings of the IEEE/CVF Conference on Computer Vision and Pattern Recognition*, pages 7210–7219, 2021. 3
- [43] Nelson Max. Optical models for direct volume rendering. *IEEE Transactions on Visualization and Computer Graphics*, 1(2):99–108, 1995. 3
- [44] Nelson Max and Min Chen. Local and global illumination in the volume rendering integral. Technical report, Lawrence Livermore National Lab.(LLNL), Livermore, CA (United States), 2005. 4
- [45] Ben Mildenhall, Peter Hedman, Ricardo Martin-Brualla, Pratul P Srinivasan, and Jonathan T Barron. Nerf in the dark: High dynamic range view synthesis from noisy raw images. In *Proceedings of the IEEE/CVF Conference on Computer Vision and Pattern Recognition*, pages 16190–16199, 2022. 2, 3
- [46] Ben Mildenhall, Pratul P Srinivasan, Matthew Tancik, Jonathan T Barron, Ravi Ramamoorthi, and Ren Ng. Nerf: Representing scenes as neural radiance fields for view synthesis. *Communications of the ACM*, 65(1):99–106, 2021. 1, 3, 6
- [47] Thomas Müller, Alex Evans, Christoph Schied, and Alexander Keller. Instant neural graphics primitives with a multiresolution hash encoding. *ACM Transactions on Graphics (ToG)*, 41(4):1–15, 2022. 3
- [48] Thomas Müller. Tiny cuda neural networks. <https://github.com/NVlabs/tiny-cuda-nn>, 2021.
- [49] Michael Niemeyer, Jonathan T Barron, Ben Mildenhall, Mehdi SM Sajjadi, Andreas Geiger, and Noha Radwan. Regnerf: Regularizing neural radiance fields for view synthesis from sparse inputs. In *Proceedings of the IEEE/CVF Conference on Computer Vision and Pattern Recognition*, pages 5480–5490, 2022. 3
- [50] Tomas Nikodym. Ray tracing algorithm for interactive applications. *BSc, Czech Technical University, Prague, Czech Republic*, 2010.
- [51] Adam Paszke, Sam Gross, Soumith Chintala, Gregory Chanan, Edward Yang, Zachary DeVito, Zeming Lin, Al-

- ban Desmaison, Luca Antiga, and Adam Lerer. Automatic differentiation in pytorch. 2017.
- [52] Adam Paszke, Sam Gross, Francisco Massa, Adam Lerer, James Bradbury, Gregory Chanan, Trevor Killeen, Zeming Lin, Natalia Gimelshein, Luca Antiga, et al. Pytorch: An imperative style, high-performance deep learning library. *Advances in neural information processing systems*, 32, 2019.
- [53] Eric Penner and Li Zhang. Soft 3d reconstruction for view synthesis. *ACM Transactions on Graphics (TOG)*, 36(6):1–11, 2017. 2
- [54] Ravi Ramamoorthi and Pat Hanrahan. On the relationship between radiance and irradiance: determining the illumination from images of a convex lambertian object. *JOSA A*, 18(10):2448–2459, 2001. 4
- [55] Konstantinos Rematas and Vittorio Ferrari. Neural voxel renderer: Learning an accurate and controllable rendering tool. In *Proceedings of the IEEE/CVF Conference on Computer Vision and Pattern Recognition*, pages 5417–5427, 2020. 2
- [56] Bernhard Riemann. On the hypotheses which lie at the foundation of geometry, translated by wk clifford. *Nature*, 8:1873, 1854. 3
- [57] Greg Schussman and K-L Ma. Anisotropic volume rendering for extremely dense, thin line data. In *IEEE Visualization 2004*, pages 107–114. IEEE, 2004. 3
- [58] Peter Shirley. Monte carlo methods for rendering. *ACM SIGGRAPH’96 Course Notes CD-ROM-Global Illumination in Architecture and Entertainment*, pages 1–26, 1996.
- [59] Sudipta Sinha, Drew Steedly, and Rick Szeliski. Piecewise planar stereo for image-based rendering. In *2009 International Conference on Computer Vision*, pages 1881–1888, 2009. 2
- [60] Vincent Sitzmann, Justus Thies, Felix Heide, Matthias Nießner, Gordon Wetzstein, and Michael Zollhofer. Deepvoxels: Learning persistent 3d feature embeddings. In *Proceedings of the IEEE/CVF Conference on Computer Vision and Pattern Recognition*, pages 2437–2446, 2019. 2
- [61] Peter-Pike Sloan, Jan Kautz, and John Snyder. Precomputed radiance transfer for real-time rendering in dynamic, low-frequency lighting environments. In *Seminal Graphics Papers: Pushing the Boundaries, Volume 2*, pages 339–348. 2023. 4
- [62] Zhenbo Song, Wayne Chen, Dylan Campbell, and Hongdong Li. Deep novel view synthesis from colored 3d point clouds. In *Computer Vision–ECCV 2020: 16th European Conference, Glasgow, UK, August 23–28, 2020, Proceedings, Part XXIV 16*, pages 1–17. Springer, 2020. 2
- [63] Pratul P Srinivasan, Tongzhou Wang, Ashwin Sreelal, Ravi Ramamoorthi, and Ren Ng. Learning to synthesize a 4d rgbd light field from a single image. In *Proceedings of the IEEE International Conference on Computer Vision*, pages 2243–2251, 2017. 2
- [64] SuLvXiangXin. Zipnerf-torch: a pytorch implementation of zipnerf. <https://github.com/SuLvXiangXin/zipnerf-pytorch>, 2023. 6
- [65] Cheng Sun, Min Sun, and Hwann-Tzong Chen. Direct voxel grid optimization: Super-fast convergence for radiance fields reconstruction. In *Proceedings of the IEEE/CVF Conference on Computer Vision and Pattern Recognition*, pages 5459–5469, 2022. 3
- [66] Dor Verbin, Peter Hedman, Ben Mildenhall, Todd Zickler, Jonathan T Barron, and Pratul P Srinivasan. Ref-nerf: Structured view-dependent appearance for neural radiance fields. In *2022 IEEE/CVF Conference on Computer Vision and Pattern Recognition (CVPR)*, pages 5481–5490. IEEE, 2022. 6
- [67] Guangcong Wang, Zhaoxi Chen, Chen Change Loy, and Ziwei Liu. Sparsenerf: Distilling depth ranking for few-shot novel view synthesis. *arXiv preprint arXiv:2303.16196*, 2023. 3
- [68] Jiepeng Wang, Peng Wang, Xiaoxiao Long, Christian Theobalt, Taku Komura, Lingjie Liu, and Wenping Wang. Neuris: Neural reconstruction of indoor scenes using normal priors. In *European Conference on Computer Vision*, pages 139–155. Springer, 2022. 2
- [69] Jinglu Wang, Bo Sun, and Yan Lu. Mvpnet: Multi-view point regression networks for 3d object reconstruction from a single image. In *Proceedings of the AAAI Conference on Artificial Intelligence*, volume 33, pages 8949–8956, 2019. 2
- [70] Yusen Wang, Zongcheng Li, Yu Jiang, Kaixuan Zhou, Tuo Cao, Yanping Fu, and Chunxia Xiao. Neuralroom: Geometry-constrained neural implicit surfaces for indoor scene reconstruction. *arXiv preprint arXiv:2210.06853*, 2022. 2
- [71] Zhou Wang, A.C. Bovik, H.R. Sheikh, and E.P. Simoncelli. Image quality assessment: from error visibility to structural similarity. *IEEE Transactions on Image Processing*, 13(4):600–612, 2004. 6
- [72] Daniel N Wood, Daniel I Azuma, Ken Aldinger, Brian Curless, Tom Duchamp, David H Salesin, and Werner Stuetzle. Surface light fields for 3d photography. In *Seminal Graphics Papers: Pushing the Boundaries, Volume 2*, pages 487–496. 2023. 2
- [73] Haoyu Wu, Alexandros Graikos, and Dimitris Samaras. S-volsdf: Sparse multi-view stereo regularization of neural implicit surfaces. *arXiv preprint arXiv:2303.17712*, 2023. 2
- [74] Liwen Wu, Jae Yong Lee, Anand Bhattad, Yu-Xiong Wang, and David Forsyth. Diver: Real-time and accurate neural radiance fields with deterministic integration for volume rendering. In *Proceedings of the IEEE/CVF Conference on Computer Vision and Pattern Recognition*, pages 16200–16209, 2022.
- [75] Huang Xin, Zhang Qi, Feng Ying, Li Hongdong, Wang Xuan, and Wang Qing. Hdr-nerf: High dynamic range neural radiance fields. *arXiv preprint arXiv:2111.14451*, 2, 2021. 3
- [76] Wenpeng Xing and Jie Chen. Mvsplenoctree: Fast and generic reconstruction of radiance fields in plenoctree from multi-view stereo. In *Proceedings of the 30th ACM International Conference on Multimedia*, pages 5114–5122, 2022. 1
- [77] Qiangeng Xu, Zexiang Xu, Julien Philip, Sai Bi, Zhixin Shu, Kalyan Sunkavalli, and Ulrich Neumann. Point-nerf: Point-based neural radiance fields. In *Proceedings of the IEEE/CVF Conference on Computer Vision and Pattern Recognition*, pages 5438–5448, 2022.

- [78] Jiawei Yang, Marco Pavone, and Yue Wang. Freenerf: Improving few-shot neural rendering with free frequency regularization. In *Proceedings of the IEEE/CVF Conference on Computer Vision and Pattern Recognition*, pages 8254–8263, 2023. [1](#), [3](#)
- [79] Lior Yariv, Jitao Gu, Yoni Kasten, and Yaron Lipman. Volume rendering of neural implicit surfaces. *Advances in Neural Information Processing Systems*, 34:4805–4815, 2021.
- [80] Alex Yu, Ruilong Li, Matthew Tancik, Hao Li, Ren Ng, and Angjoo Kanazawa. Plenoctrees for real-time rendering of neural radiance fields. In *Proceedings of the IEEE/CVF International Conference on Computer Vision*, pages 5752–5761, 2021.
- [81] Kai Zhang, Gernot Riegler, Noah Snavely, and Vladlen Koltun. Nerf++: Analyzing and improving neural radiance fields. *arXiv preprint arXiv:2010.07492*, 2020. [2](#), [4](#)
- [82] Richard Zhang, Phillip Isola, Alexei A Efros, Eli Shechtman, and Oliver Wang. The unreasonable effectiveness of deep features as a perceptual metric. In *Proceedings of the IEEE conference on computer vision and pattern recognition*, pages 586–595, 2018. [6](#)
- [83] Xuanmeng Zhang, Zhedong Zheng, Daiheng Gao, Bang Zhang, Pan Pan, and Yi Yang. Multi-view consistent generative adversarial networks for 3d-aware image synthesis. In *Proceedings of the IEEE/CVF Conference on Computer Vision and Pattern Recognition*, pages 18450–18459, 2022. [2](#)
- [84] Tinghui Zhou, Richard Tucker, John Flynn, Graham Fyffe, and Noah Snavely. Stereo magnification: Learning view synthesis using multiplane images. *arXiv preprint arXiv:1805.09817*, 2018. [2](#)